Arabian Journal for Science and Engineering (2023) 48:16769–16782
https://doi.org/10.1007/s13369-023-08078-z

RESEARCH ARTICLE-PETROLEUM ENGINEERING

Internal Flow Simulation and Experimental Study of Non-moving Component Jet Oscillation Tool

Jialin Tian[1] · Lanhui Mao[1] · Chenghang Liu[1] · Haolin Song[1] · Junyang Song[1]

Received: 1 March 2023 / Accepted: 18 June 2023 / Published online: 6 July 2023

Abstract
Aiming at the problems of high drilling friction and serious backing pressure on the drill string under the difficult oil and gas drilling conditions, which leads to low rate of penetration(ROP) or low rock-breaking efficiency, this article proposed a non-moving component jet oscillation tool based on the Coanda effect. Combined with the field working conditions of drilling process, the numerical simulations of the oscillation nipple internal flow are completed first. After that, the recirculation characteristics, switching mechanism and entrainment effect of the internal fluid are studied, including the flow velocities and the dynamics features of the pressure field at different positions. The experimental tests are conducted to verify the theoretical study results. The results show that the fluid presents same periodic wall-attached and switching behaviors. With the inlet flow increasing, the fluid velocities at the inlet and outlet locations show quasi-linear distributions, and the fluid pressures loss changes periodically. The jet oscillation tool can generate appropriate periodic pressure pulse, and the pulse value and fluid switching period are determined by design parameters. The comparative analysis between numerical simulations and experimental tests shows the results exhibit similar characteristics. It is concluded that this non-moving component tool can produce periodic oscillation effect, thereby changing the friction status between the drilling tools and wellbore and improving drilling efficiency. The research results can provide references for optimization designs of similar downhole tools and also develop technical supports for the efficient exploitation of oil and gas resources.

Keywords Drilling friction · Backing pressure · Jet oscillation · No-moving component · Pressure pulse

1 Introduction

With the increase in the energy demands, unconventional oil and gas resources such as shale gas, coalbed methane and gas hydrate have been developed to compensate the shortage of oil and gas productions. In the exploitation process of unconventional resources, the long displacement or horizontal well technology is becoming more mature, which makes the drilling engineering facing more difficulties such as large friction problem [1]. Especially in the long horizontal sections, the sliding drilling is adopted and contact area is increased between drill string and borehole wall. When the horizontal well section extends far, the self-weight direction of drill string deviates from the horizontal axis. The transfer efficiency of weigh on bit (WOB) is low [2, 3]. Meanwhile, due to the formation difference and the accumulation of cutting bed, the drilling friction in the horizontal well is much larger than that of the vertical well, which leads to the negative influences, including the high backing pressure, the low rate of penetration (ROP), even the drill string buckling, stick–slip, etc. [4, 5].

Reducing the drilling friction and improving drilling efficiency have become a challenge in drilling engineering. The scholars in drilling industry throughout the world have carried out a lot of research. The current friction reduction tools usually use axial or circumferential impact to transform the hydraulic energy of drilling fluid into the mechanical energy of the tool, which causes the tool to vibrate. By adding these tools into the drilling assembly, it can effectively reduce drilling friction and improve drilling efficiency [6, 7]. The axial friction reduction tools can generate axial vibration, form axial impact force, change the force status of drill string and achieve friction reduction. Related tools include hydraulic oscillators, etc. [8]. The circumferential

✉ Lanhui Mao
maolanhui01@163.com

[1] Oil and Gas Equipment Technology Sharing and Service Platform of Sichuan Province, School of Mechanical Engineering, Southwest Petroleum University, Chengdu 610500, Sichuan, China

friction reducing tool generates periodic torque and transmits it to drill bit to assist rock breaking, which can improve the rock-breaking efficiency. Related tools include rotary impact speed-up tool, torsional impactor, etc. [9]. Rasheed [10] first proposed a hydraulic oscillator; the fluid action of the tool creates pressure pulses. These pulses oscillate the bottom hole assembly (BHA), reducing friction and improving weight transfer. Newman et al. [11] studied the effect of the circumferential and axial vibration on the drilling friction, which the vibration between drill string and borehole can be reduced by applying additional vibration. Al-Buali et al. [12] studied the effect of the oscillator, the extended length of horizontal well section is increased, and drilling friction is reduced when the drill string system was added to the hydrodynamic oscillator. Barton [13] and others illustrated case studies from field application, where the Drilling Agitator Tool (DAT) has proved to help reduce torque and stick–slip and improve the transmission efficiency of the WOB. Based on the sliding drilling principle, Li et al. [14] revealed that bottom hole assembly (BHA) with hydraulic oscillator reduces the sliding friction between the drilling string and wellbore by creating hydraulic vibration, thus improving the transfer efficiency of WOB. Dong [15] discusses the working mechanism of the hydraulic oscillator, and numerical calculation and experimental verification of operation parameters of the oscillator are conducted. Wang et al.[16] established the vibration reduction model for high-angle wells and explore the influence factors of drilling friction. Comparative analysis of axial and lateral vibration models is carried out by Gee et al. [17] to verify that axial vibration is more effective in reducing the drilling friction. Panda et al. [18] investigated effect of the nature of vitiated crossflow on the structure and dynamics of non-reacting/reacting transverse jets. Tian et al. [19] studied the dynamics and vibration characteristics of a new type of jet vibration friction reduction tool in horizontal well and verified its correctness through experiments. Hsu [20] and others experimentally studied the flow and heat transfer characteristics of a pulsed jet impinging on a flat plate under various excitation conditions.

However, the current downhole vibration friction-reducing tools expose many problems during drilling processes, such as great loss of working pressure due to its complex structure, poor erosion resistance and vulnerability to formation environment. These problems can reduce tool life and even cause failure, and affect drilling production. Therefore, in order to overcome the above problems, we propose a jet oscillation tool with non-moving components. This tool relies on the automatic switching of the fluid in the circulating flow channel to generate oscillation effect and achieve the function of reducing friction and drag.

Combining with the field working condition parameters, the numerical simulations of oscillation nipple internal flow are completed. The recirculation characteristics, switching mechanism and entrainment effect of the internal fluid are studied, including the flow velocities and the dynamics features of the pressure field at different positions. Especially, the influences of initial boundary conditions on working characteristics are carried out based on the drilling circulating medium of this tool. Finally, the experimental research is carried out to complete the experimental test of the working parameters of the new tool, and the experimental test and numerical simulation results are compared to verify the accuracy of theoretical researches.

2 Structure Mechanism

The non-moving component jet oscillation tool is composed of shock absorber and oscillator. The shock absorber mainly consists of upper joint, damping shaft and mandrel. The oscillator consists of conversion connector, oscillation nipple and the case. The lower end of the oscillator is connected to the polycrystalline diamond composite (PDC) drill bit through lower joint, and the structure design is as shown in Fig. 1. The drilling fluid flows through the upper joint, damping shaft and the hollow hole in mandrel of shock absorber assembly to the bottom oscillator assembly and generates a high-speed and uniform jet through the nozzle at the inlet of the oscillation nipple. The drilling fluid circulates in the oscillation nipple to achieve oscillation periodically. During the working process, the tool will generate periodic pulse pressure waves, which will be transmitted to the shock absorber. Under the action of the pulse pressure, the elastic component inside the shock absorber periodically compresses and resets, causing the tool to generate periodic axial vibration. Thus, the friction conditions between drill string and borehole can be improved by the vibration energy.

In the initial stage, the main jet flow is uniform in the oscillation nipple, and the pressure on both sides of jet is symmetrically distributed. Due to jet diffusion and splitter effect, the pressure loss on both sides of main jet begins to be unbalanced, and the jet flows toward the expansion wall that has a small pressure until the main jet is completely adsorbed on the expansion wall. The internal flow channel structure and fluid circulation route of the oscillation nipple are shown in Fig. 2. Using the principle of Coanda effect, the main jet flow can form a pressure fluctuation by switching between the two steady statuses. The main jet flows through the upper input channel into the oscillation chamber and forms a clockwise vortex and then flows out through the fluid outlet, which is the upper steady status of the fluid circulation. The main jet flow through the lower input channel flows into the oscillation chamber and forms a counterclockwise vortex, and then flows out through the fluid outlet, which is the lower steady status. The reverse feedback is performed by the control flow flowing out from the feedback channel to push the main jet to

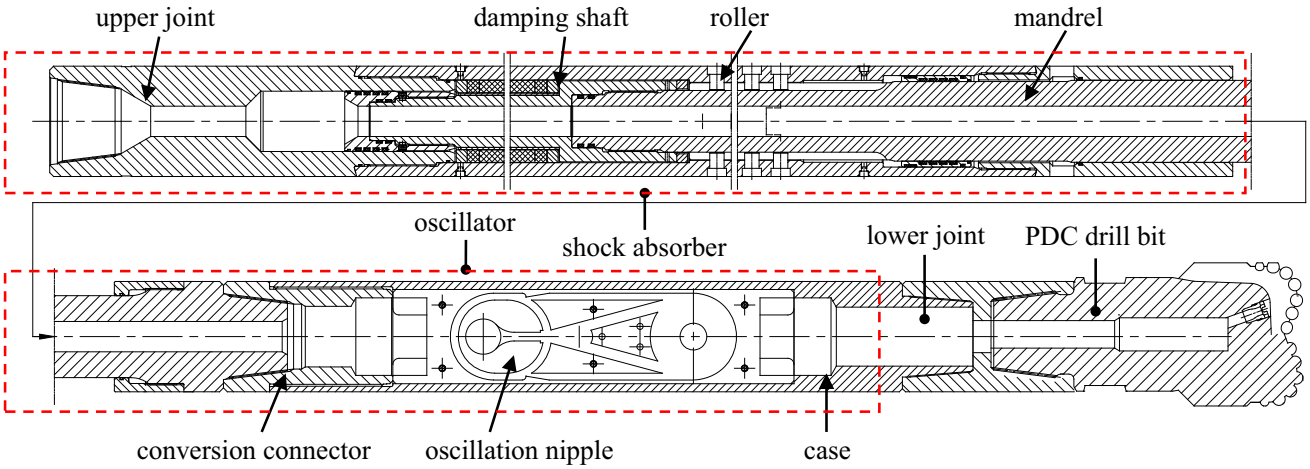

Fig. 1 Structure composition of non-moving component jet oscillation tool

Fig. 2 Internal fluid circulation of oscillation nipple

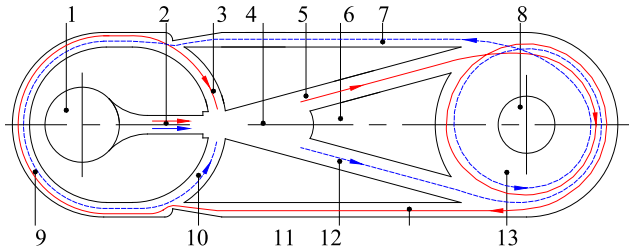

1-fluid inlet, 2-jet nozzle, 3-upper control channel, 4-jet chamber, 5-upper input channel, 6-spliter, 7-upper feedback channel, 8-fluid outlet, 9-common channel, 10 - lower control channel, 11-lower input channel, 12-lower feedback channel, 13-oscillation chamber

change the wall-attached direction. The jet oscillation can be formed by switching between the two steady statuses. With the action of the shock absorber, the jet oscillation tool can generate periodic axial vibration, which converts the static friction between drill string and borehole wall into dynamic friction to realize vibration antifriction and resistance reduction.

3 Theoretical Formulation and Boundary Conditions

3.1 Theoretical Formulation

Assume the fluid is incompressible, has constant physical properties, ignoring the body-force on the fluid and does not exchange heat with the outside. Reynolds-averaged Navier–Stokes and continuity equations are used as the control equations. The RNG k–ε turbulence model is used. The Reynolds-averaged N-S equation is obtained by time-averaging the N-S equation, as shown below [21].

$$\begin{cases} \dfrac{\partial p}{\partial t}+\dfrac{\partial}{\partial x_i}(\rho\overline{u}_i)=0 \\ \dfrac{\partial}{\partial t}(\rho\overline{u}_i)+\dfrac{\partial}{\partial x_j}\left(\rho\overline{u}_i\overline{u}_j\right)=-\dfrac{\partial\overline{p}}{\partial x_i} \\ \quad +\dfrac{\partial}{\partial x_j}\left[\mu\left(\dfrac{\partial\overline{u}_i}{\partial x_j}+\dfrac{\partial\overline{u}_j}{\partial x_i}-\dfrac{2}{3}\delta_{ij}\dfrac{\partial\overline{u}_k}{\partial x_k}\right)\right]+\dfrac{\partial}{\partial x_j}\left(-\rho\overline{u}_i'\overline{u}_j'\right) \end{cases} \tag{1}$$

where ρ is the density, kg/m^3; t is the time, s; x_i, x_j, x_k are component symbols, respectively ($i = 1, 2, 3$; $j = 1, 2, 3$; $k = 1, 2, 3$); $\overline{u}_i$, $\overline{u}_j$, $\overline{u}_k$ are the Reynolds-average velocity components, respectively; μ is the dynamic viscosity, Pa·s; $\overline{p}$ is the average pressure, MPa; $\overline{u}_i'$, $\overline{u}_j'$ is the average fluctuation velocity components, respectively; δ_{ij} is the Kronecker tensor component.

Through the Boussinesq assumption, the Reynolds stress can be related to the average velocity gradient, and the Reynolds stress model is

$$-\rho\overline{u}_i'\overline{u}_j'=\mu_t\left(\frac{\partial\overline{u}_i}{\partial x_j}+\frac{\partial\overline{u}_j}{\partial x_i}\right)-\frac{2}{3}\left(\rho k+\mu_t\frac{\partial\overline{u}_l}{\partial x_l}\right)\delta_{ij} \tag{2}$$

where the turbulent viscosity μ_t is

$$\mu_t = \rho C_\mu \frac{k}{\varepsilon} \tag{3}$$

In the above equations, k is the turbulence kinetic energy, ε is the turbulent dissipation, C_μ is the constant.

The RNG k–ε turbulence model is as follows [22].

The kinetic energy equation is

$$\frac{\partial(\rho k)}{\partial t} + \frac{\partial(\rho k u_i)}{\partial x_i} = \frac{\partial}{\partial x_j}\left(\alpha_k \mu_{\text{eff}} \frac{\partial k}{\partial x_j}\right) + G_k + G_b - \rho\varepsilon - Y_M + S_k \tag{4}$$

The dissipation equation is

$$\frac{\partial(\rho\varepsilon)}{\partial t} + \frac{\partial(\rho\varepsilon u_i)}{\partial x_i} = \frac{\partial}{\partial x_j}\left(\alpha_\varepsilon \mu_{\text{eff}} \frac{\partial \varepsilon}{\partial x_j}\right) + C_{1\varepsilon}\frac{\varepsilon}{k}(G_k + C_{3\varepsilon}G_b) - C_{2\varepsilon}\rho\frac{\varepsilon^2}{k} - R_\varepsilon + S_\varepsilon \tag{5}$$

in which G_k, G_b and Y_M are the generation terms of turbulent kinetic energy caused by average velocity gradient, buoyancy and pulsation expansion, respectively, $C_{1\varepsilon}$, $C_{2\varepsilon}$ and $C_{3\varepsilon}$ are the empirical constants. α_k and α_ε are the Prandtl numbers corresponding to turbulent kinetic energy and dissipation rate, respectively. S_k,S_ε and μ_{eff}, R_ε are the user-defined parameters and correction parameters, respectively.

3.2 Boundary Conditions

The inlet of the computational model is defined as the velocity boundary condition, the outlet is defined as the pressure outlet, and the outlet pressure is defined as atmosphere. The model inlet and outlet turbulence intensity and hydraulic diameter can be calculated by the following equations [23, 24].

$$\begin{cases} I = 0.16(\text{Re})^{-1/8} \\ \text{Re} = \dfrac{\rho u D_e}{\mu} \\ D_e = \dfrac{4A}{C} \end{cases} \tag{6}$$

where I is the turbulence intensity, Re is the Reynolds number, ρ is the fluid density, kg/m^3, u is the flow velocity, m/s, μ is the dynamic viscosity, Pa·s, D_e is the hydraulic diameter, m, A is the flow area, m^2, C is the perimeter of cross section, m.

The fluid working medium is set to clean water that the density is 998.2 kg/m^3 and the dynamic viscosity is 0.001 Pa·s. With the same calculation grid and different inlet flow conditions [25] (5, 9, 17, 25 L/s), the numerical simulation of the internal flow of the jet oscillation tool is carried out. The boundary condition parameters are shown in Table 1.

4 Numerical Simulation and Result Analysis

4.1 Jet Wall-Attached Simulation

Taking the velocity nephogram when the inlet flow rate is 5L/s as an example, the wall-attached and switching process of the internal fluid is shown in Fig. 3. In the initial stage, the upper and lower input channels are symmetrically distributed, and the control pressures are identical. The jet flow is in free status and the main jet flow enters the oscillation chamber along the upper and lower input channels, as shown in Fig. 3a. Under the influence of jet diffusion and splitter, the jet flows toward the small pressure wall and enters the oscillation chamber through the upper input channel, as shown in Fig. 3b. Under the pressure difference effect, the deflection of jet flow continues to increase until it is completely wall attached, which is shown in Fig. 3c. The oscillation chamber begins to form a vortex and part of the fluid enters the lower feedback channel. As the fluid entering the upper input channel increases, a stable flow is formed in a short time, as shown in Fig. 3d, the jet forms a clockwise vortex in the oscillation chamber, and back pressure rises. Under the action of upper control flow, the upper side pressure is greater than the lower side pressure of the main jet flow; the jet flow begins to detach and switch direction, as shown in Fig. 3e. When the jet flow converts from the upper input channel to the lower, the switching process is completed, which is shown in Fig. 3f. As the fluid in the lower input channel continues to increase, a stable Coanda flow is formed, and a counterclockwise vortex is formed in the oscillating chamber, as shown in Fig. 3g. After that, the vortex intensity is stronger, the back pressure is greater, and the jet is gradually strengthened, as shown in Fig. 3h. The jet flow completes a cycle of the wall attachment and switching process in the oscillation nipple.

4.2 Velocity Analysis

When the fluid simulation results are post-processed, the flow velocity results can be obtained which are shown in Fig. 4. The velocity streamline diagram shows the presence of the Coanda flow and entrainment in the oscillation nipple. The inlet flow rate is 5L/s and 9L/s; the fluid evenly adheres to the lower wall, enters the oscillation chamber from the lower input channel and forms a counterclockwise vortex in the oscillation chamber, while for 17L/s and 25L/s, the fluid in

Table 1 Outlet and inlet conditions under different input flows

Quantity of flow (L/s)	5	9	17	25
Inlet diameter (m)	0.05			
Inlet area (m^2)	3.927×10^{-3}			
Inlet velocity (m/s)	1.27	2.29	4.33	6.37
Inlet hydraulic diameter (m)	0.05			
Inlet Reynolds number	63,357	114,043	215,415	316,787
Inlet turbulence intensity	4.02%	3.73%	3.45%	3.28%
Outlet diameter (m)	0.04			
Outlet area (m^2)	2.51×10^{-3}			
Outlet turbulence intensity	3.91%	3.63%	3.35%	3.19%
Outlet hydraulic diameter (m)	0.04			

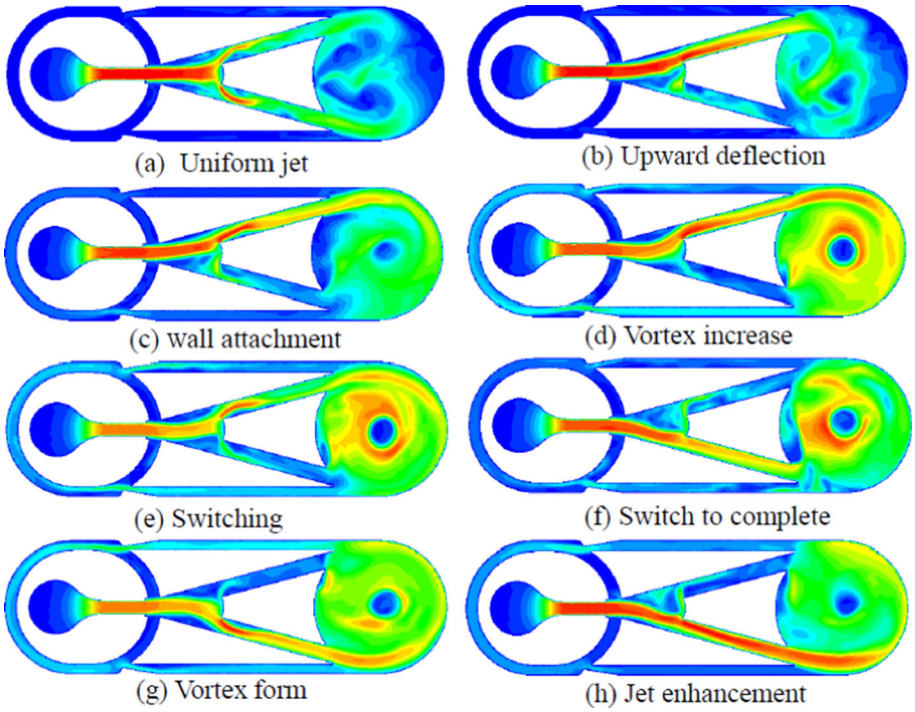

Fig. 3 Wall attachment and switching process of the internal fluid

the channel is in switching process. At this time, the oscillation chamber does not form a complete vortex, and the fluid in the oscillation chamber is relatively turbulent.

The relationship between the outlet and inlet velocity and the inlet flow rate can be obtained as shown in Fig. 5. Due to the difference between the inlet and outlet areas, the flow velocity is small at the inlet location. As the fluid is ejected from the nozzle, the jet flow is wall attached in the channel and forms a vortex in the oscillation chamber. With inlet flow rate increases, the outlet velocity is greatly improved compared with the inlet. The inlet flow rate increases from 5 to 25L/s, and the inlet velocity increases from 1.27 to 6.37 m/s. The outlet velocity also increases which presents basically a quasi-linear distribution.

4.3 Pressure Loss Analysis

Figure 6 shows the characteristic curves of the pressure, which include the locations of the fluid inlet and outlet, the upper and lower input channels, and the upper and lower control channels. In the initial stage, the pressure at each monitoring location keeps rising. When the jet has a Coanda oscillation, the tool starts to work normally and the pressure at each monitoring location begins to show obvious periodic fluctuations. The central location is relatively close to inlet location, the pressure fluctuation range and cycle are little different, while the pressure fluctuation is relatively stable at outlet location. When the inlet flow rate is 5L/s, the pressure value at the inlet of oscillation nipple fluctuates in the range of 0.16 ~ 0.49 MPa, the center pressure fluctuates in

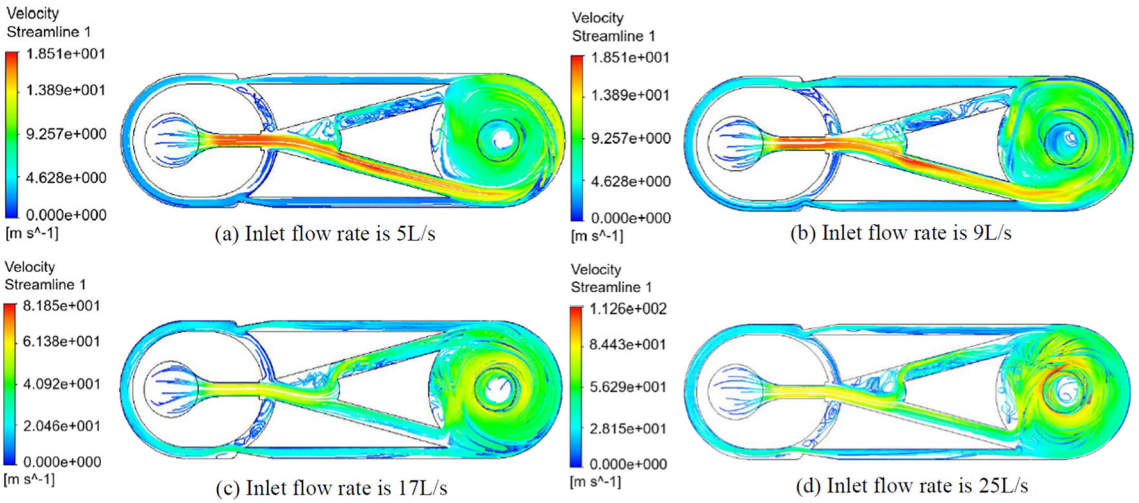

Fig. 4 Flow velocity results at different inlet flow rates

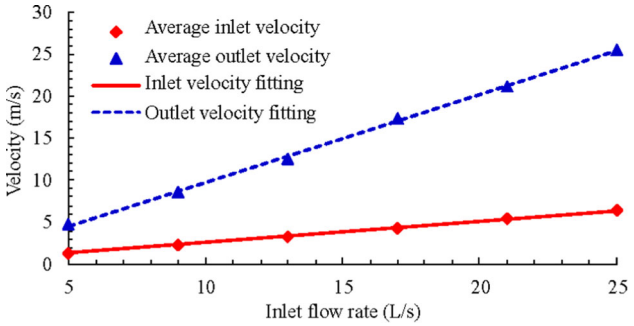

Fig. 5 Relationship between the velocity and inlet flow rate

the range of 0.05 ~ 0.49 MPa, and the pressure at the outlet fluctuates in the range of 0 ~ 0.05 MPa. The fluctuation range of tool pressure loss is 0.15 MPa ~ 0.45 MPa, and the average change period is approximately 0.12 s. When the inlet flow rate increases to 25L/s, the pressure value at the inlet of oscillation nipple fluctuates in the range of 4 ~ 13 MPa, the center pressure fluctuates in the range of 1 ~ 13 MPa, and the pressure at the outlet fluctuates in the range of 0 ~ 1.1 MPa. The tool pressure loss fluctuated from 4 to 12 MPa, and the average change period was approximately 0.08 s. The simulation results show that the pressure loss of this tool will be raising while the volumetric flow rate is increasing, and the periodic variation trend of the fluid is more obvious.

Combining with the pressure simulation calculation results, the change features of the fluid inlet and outlet pressures and pressure loss are shown in Fig. 7. When the fluid enters the oscillation nipple from the inlet, the pressure is relatively large, and it increases nonlinearly with the change of inlet flow rate. The fluid wall attached and forms a vortex in the oscillation chamber; the pressure changes continuously. The fluid pressure that flows out through outlet location is greatly reduced, which is showing an approximate quasi-linear distribution.

4.4 Flow Characteristics Analysis

The fluid flow characteristics at key locations of the oscillation nipple are analyzed, which include the upper and lower input channels, the upper and lower control channels, and the outlet location.

When the inlet flow rate is 5L/s, the characteristic curve is shown in Fig. 8. In the initial stage, the main jet flow is in a free status and the flow velocity in the upper and lower input channels has no obvious regularity. When the main jet flow starts to deflect upward, the flow velocity in the upper input channel begins to be greater than lower input channel and continuously increases. Then, the flow rate begins to decay and decreases to 0 in the lower input channel, and then starts to rise until the upper and lower input channels are equal. The fluid is in the upper wall-attached phase from 0.23 to 0.34 s. With the formation and attenuation of the vortex in the oscillation chamber, the jet flow gradually starts to deflect downward after the 0.34 s. The flow velocity in the lower input channel begins to be greater than upper input channel, continuously rises to 17 m/s and then begins to decrease. After the flow rate in the upper input channel is reduced to 0, the flow starts to rise until the flow velocity in upper and lower input channels is about equivalent at about 0.45 s. The fluid in the lower wall-attached phase is in the range of 0.34–0.45 s. The flow rate in the upper and lower input channels changes periodically, but the changing trend is opposite. The initial deflection time is 0.23 s, and the velocity value fluctuates within the range of 0 ~ 18 m/s. In addition, the average cycle of fluid wall-attached and switching process is approximately 0.24 s.

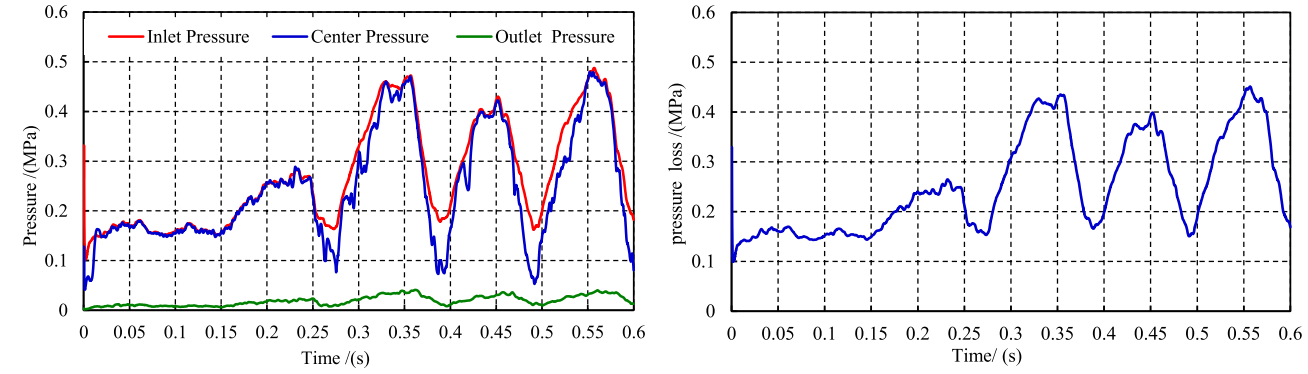

(a) The inlet flow rate is 5L/s

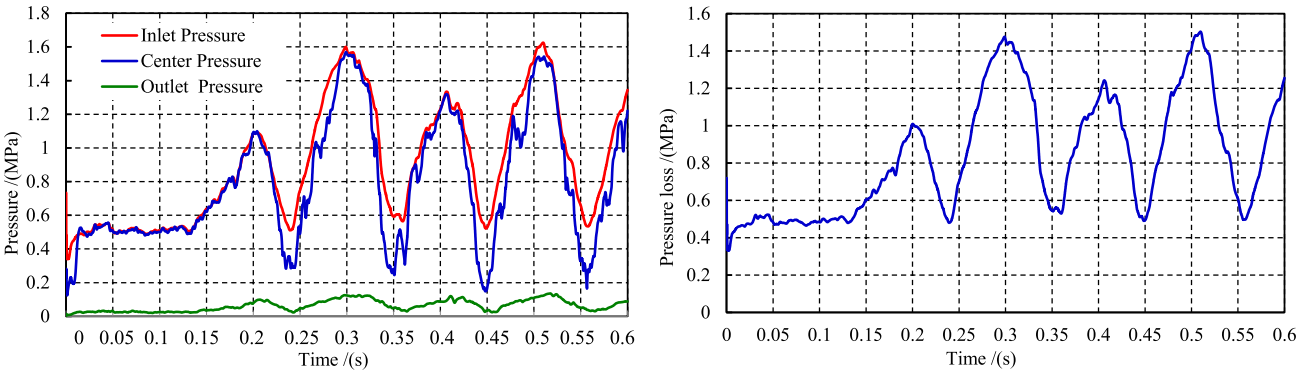

(b) The inlet flow rate is 9L/s

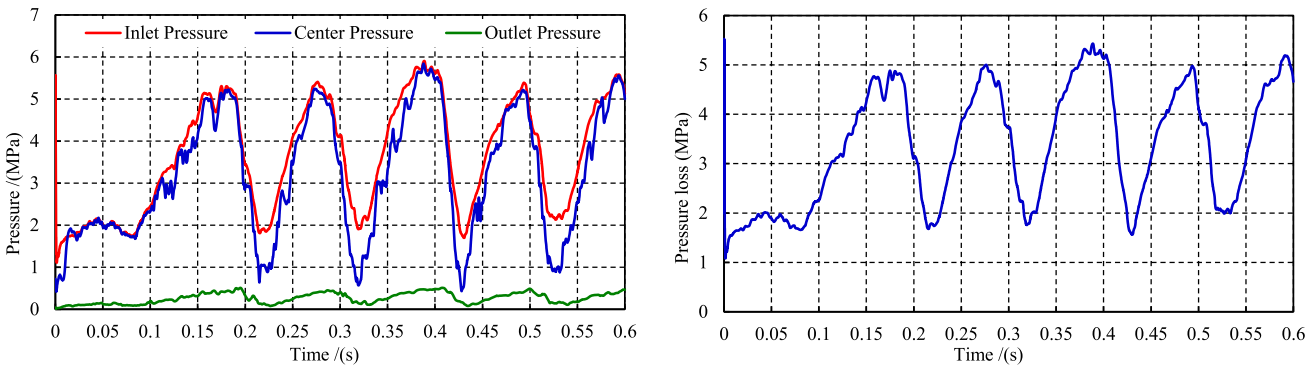

(c) The inlet flow rate is 17L/s

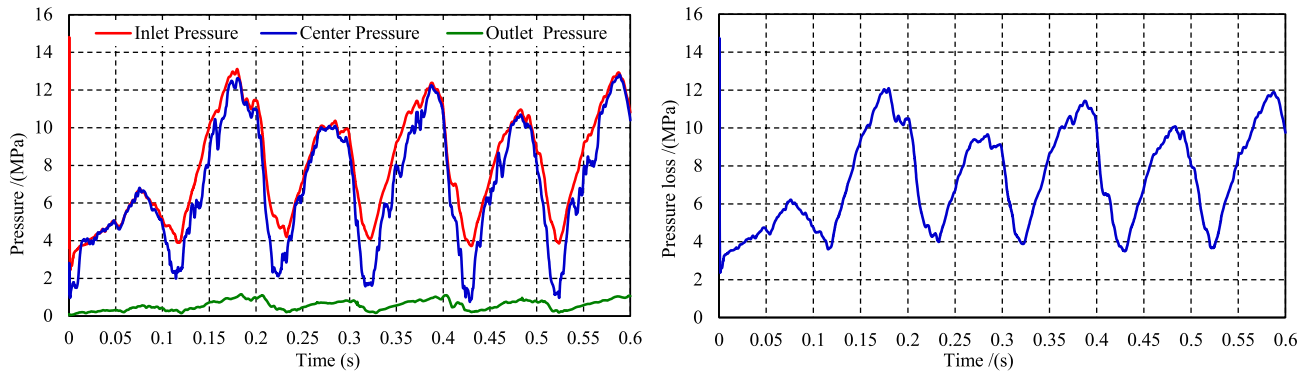

(d) The inlet flow rate is 25L/s

Fig. 6 Pressure characteristic curves at different inlet flow rates

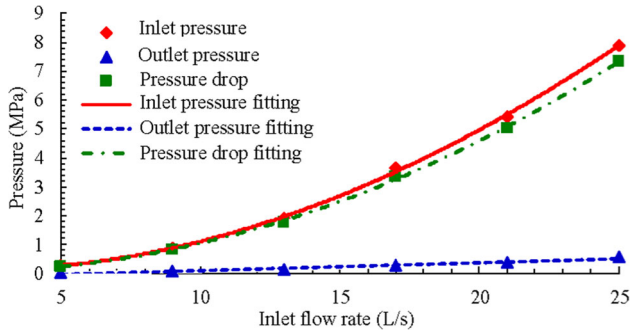

Fig. 7 Change features of the fluid inlet and outlet pressures and pressure loss

It can be seen from Fig. 8b that when the pressure in the lower control channel is greater than the upper, the main jet flow deflects upward under the pressure difference. The pressure in the upper input channel is gradually larger than lower. When the fluid begins to stabilize and be wall attached, the pressure loss is at a minimum in the cycle. When the fluid begins to be wall attached, most of the main jet flow enters the oscillation chamber from the upper input channel, and the vortex does not form in the oscillation chamber and the back pressure is low. The fluid enters the oscillation chamber, and directly flows out from outlet location. The fluid receives the least resistance and loss, that is, the pressure loss is minimum. With the formation and enhancement of the vortex in the oscillation chamber, the back pressure and pressure loss continuously increase. At the 0.34 s, the main jet flow in the oscillation nipple begins to switch. The pressure loss is at the maximum position in the cycle. The main jet flow vertically impacts splitter. Then, the jet flow enters the oscillation chamber by the upper and lower input channels to impact each other. The flow resistance and loss of the fluid are greater than wall-attached phase; the pressure loss is also greater.

When the inlet flow rate is 9L/s, the fluid flow characteristic curve is shown in Fig. 9. As shown in Fig. 9a, the time of 0 ~ 0.14 s is the initial stage and 0.14 ~ 0.21 s and 0.21 ~ 0.32 s are the lower and upper wall-attached stages, respectively. The flow rate in the upper and lower input channels changes periodically, and the velocity value fluctuates within the range of 0 ~ 34.5 m/s; the changing trend of the flow velocity in the upper and lower input channel is opposite. The velocity value at the outlet varies from 5 to 12.5 m/s which is different from the input channel. The average variation period of the outlet velocity is about 0.12 s, which is the half period of velocity change in the upper and lower input

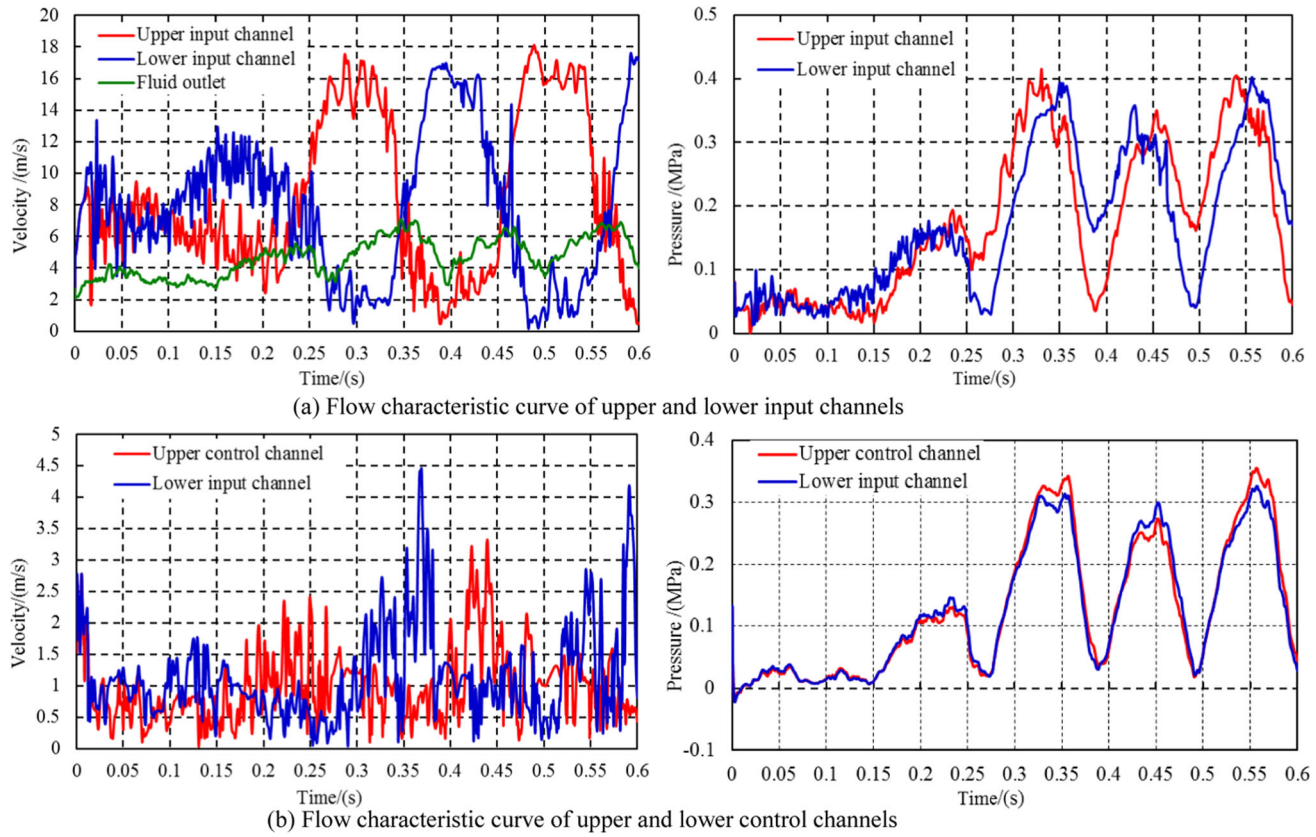

Fig. 8 Fluid flow characteristic curve of inlet flow rates (5L/s)

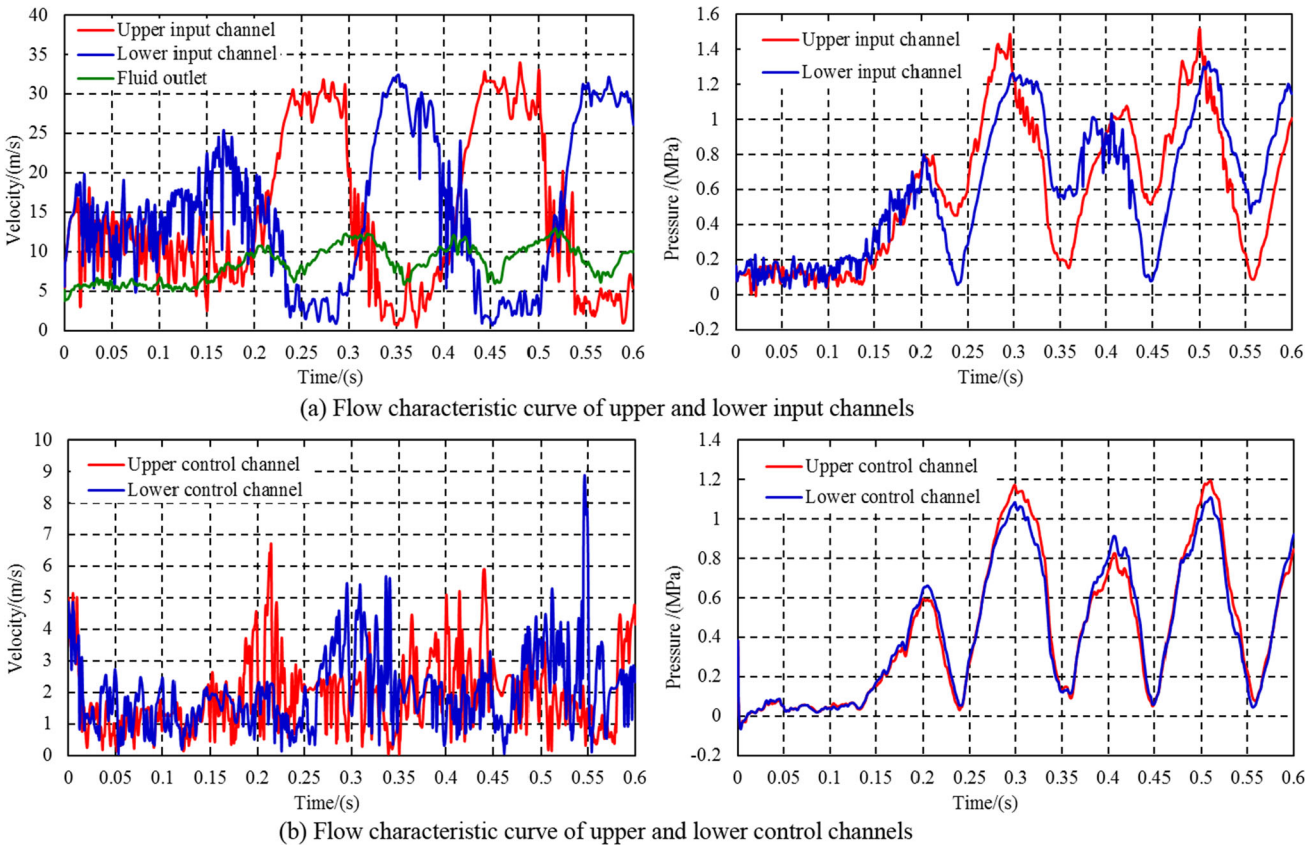

(a) Flow characteristic curve of upper and lower input channels

(b) Flow characteristic curve of upper and lower control channels

Fig. 9 Fluid flow characteristic curve of inlet flow rates (9L/s)

channels. It can be seen from Fig. 9b that the fluid velocity of the control channel in the initial stage has no obvious regularity, and then, velocity in the upper and lower control channels begins to change periodically. Velocity in the upper control channel is within the fluctuation range of 0 ~ 6.8 m/s, while lower fluctuates within the range of 0 ~ 9 m/s, which is consistent with the change period of the input channel flow rate.

When inlet flow rate is 17L/s, the characteristic curves of flow rate of each monitoring position in the oscillation nipple are shown in Fig. 10. As shown in Fig. 10a, the time of 0 ~ 0.07 s is the initial stage; 0.07 ~ 0.18 s and 0.18 ~ 0.27 s are the upper and lower wall-attached stage, respectively. The velocity value in the lower input channel fluctuates within the range of 0 ~ 60 m/s, and the average period of the wall-attached and switching is approximately 0.2 s. The outlet velocity also changes periodically and the speed fluctuation range is 10 ~ 25 m/s, and the average change period of the outlet velocity is about 0.1 s. From Fig. 10b, the velocity in the upper and lower control channels also changes periodically and shows the opposite change trend. The velocity fluctuation range is 0 ~ 15 m/s in the upper control channel while lower within the range of 0 ~ 18 m/s.

When input flow rate is 25L/s, the flow velocity variation characteristic curves are shown in Fig. 11. As shown in Fig. 11a, the time of 0 ~ 0.06 s is the initial stage, after which the wall-attached and switching phenomenon occurs. The velocity values in the upper and lower input channels fluctuate within the range of 0 ~ 90 m/s, and the average period of the wall-attached and switching is approximately 0.16 s. The outlet velocity fluctuates from 10 to 30 m/s, and the average variation period is about 0.08 s. According to Fig. 11b, the velocity in the upper and lower control channel fluctuates within the range of 0–18 m/s and the average change period is approximately 0.16 s. The pressure in the upper and lower input channels fluctuates within the range of 0.6 ~ 11 MPa and the pressure in the upper and lower control channels fluctuates within the range of 0.1 ~ 10 MPa, while the fluctuation range of the tool pressure falls from 4 to 12 MPa. The change period of the pressure loss is approximately 0.08 s, which is consistent with the average change cycle of the outlet velocity.

From the above analysis of the fluid flow characteristics in the oscillation nipple, the initial deflection time of jet flow is gradually shortened from 0.23 to 0.06 s with inlet flow increases. The periodic trend of wall attached and switching

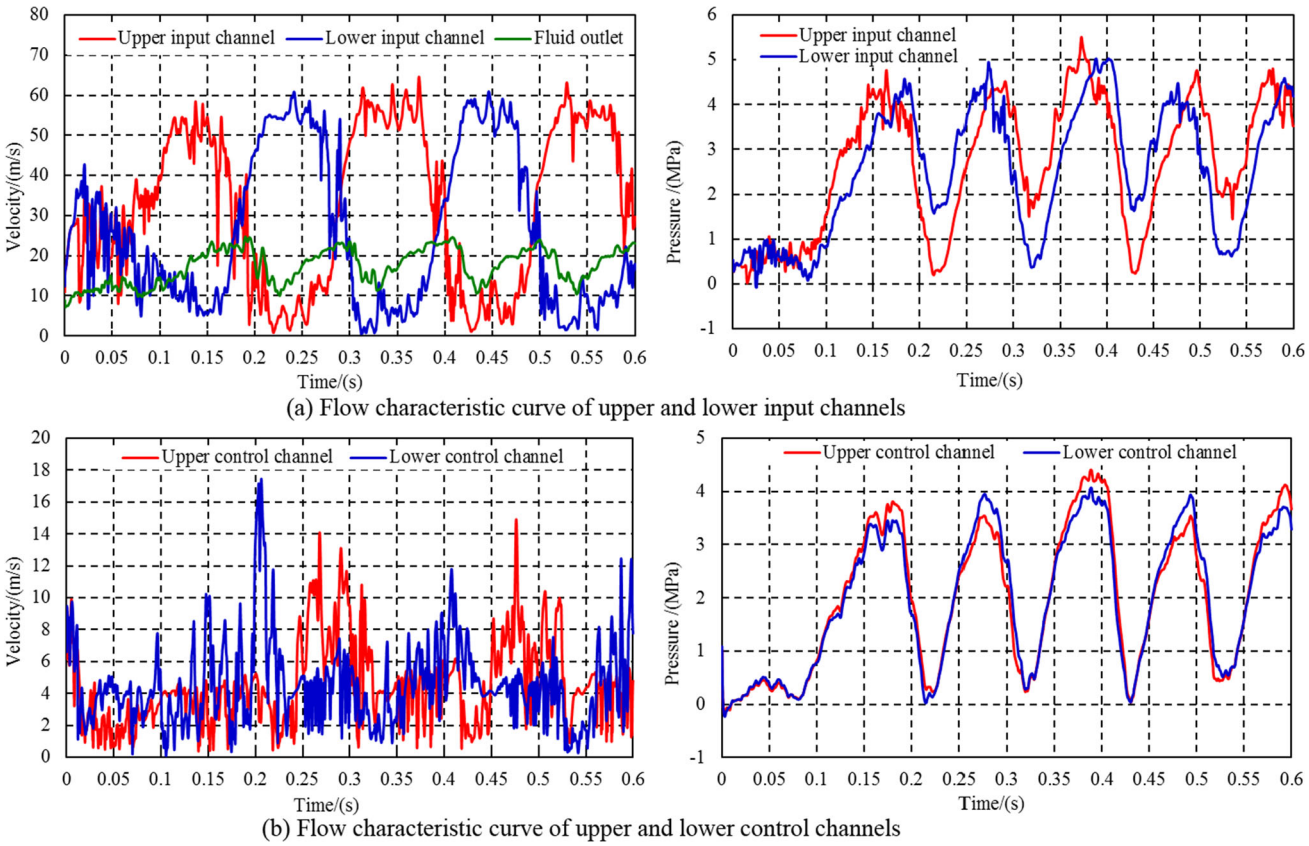

Fig. 10 Fluid flow characteristic curve of inlet flow rates (17L/s)

is more significant, and switching cycle is also gradually shortened.

5 Experimental Research

In order to verify the rationality of the structural design of non-moving component jet oscillation tool and accuracy of theoretical study results, experimental research is carried out. The experimental test system is shown in Fig. 12. The test system mainly includes water tank, horizontal centrifugal pump, various stages of valves, non-moving component jet oscillation tool, high and low pressure pipelines, etc. The double pump is used to supply the working fluid, which is pumped to the exit master valve and high pressure pipeline through pump 1 and pump 2, and enters the jet oscillation tool. Then, fluid flows into the low pressure line from the outlet end of the tool and finally flows back into the water tank. In the actual test process, to maintain the consistency with the simulation conditions, the working fluid uses clean water. The acceleration sensor, displacement sensor, pressure sensor, data acquisition device and computer (acquisition software) are connected to the test system. The flow and pressure can be controlled and adjusted through the flow and pressure regulation control platform; the circulating flow adjustment range is 5 ~ 25L/s.

A test bench is designed for this experimental test, which mainly includes pressurized mechanism, connecting rod, supports and baffles and is shown in Fig. 13. The experimental procedures are as follows: install the tool between the baffles on both sides of the experimental bench, adjust the compression nut of the experimental bench, add pre-pressure to the tool and then connect the acceleration sensor, data acquisition equipment and computer to the test system. Start pump 1 and circulate at a small flow rate to check whether the test system meets the experimental requirements, and at the same time check whether each sensor and data acquisition equipment can transmit signals and collect data normally. Adjust the input flow according to the experimental conditions in Table 2, and collect data on its working status after the jet oscillation tool works smoothly.

The two acceleration sensors are, respectively, mounted on two different positions of the tool, connecting with the data acquisition equipment and the computer to test the axial vibration acceleration. We take the stable value as analysis object, and the sampling frequency is 256 Hz. The acceleration test results under different flow rate conditions are

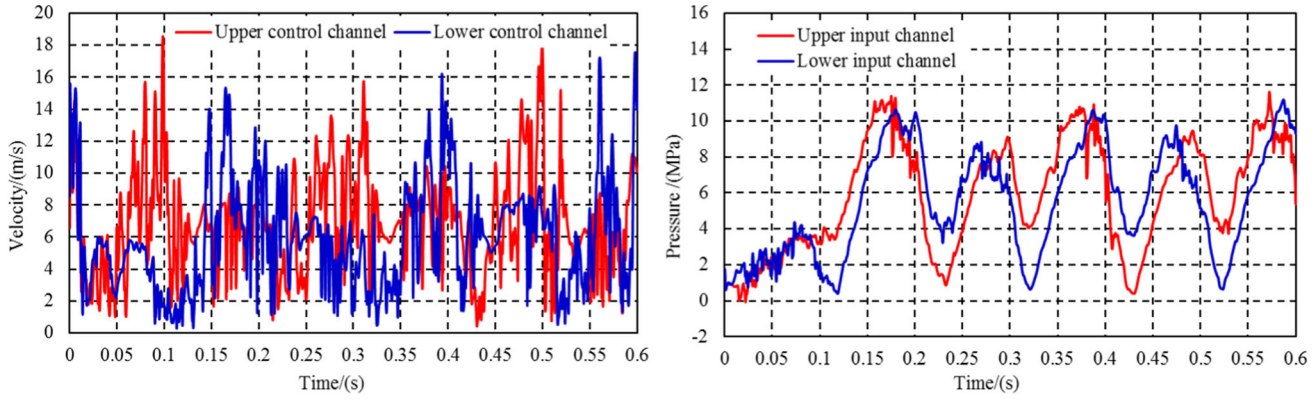

(a) Flow characteristic curve of upper and lower input channels

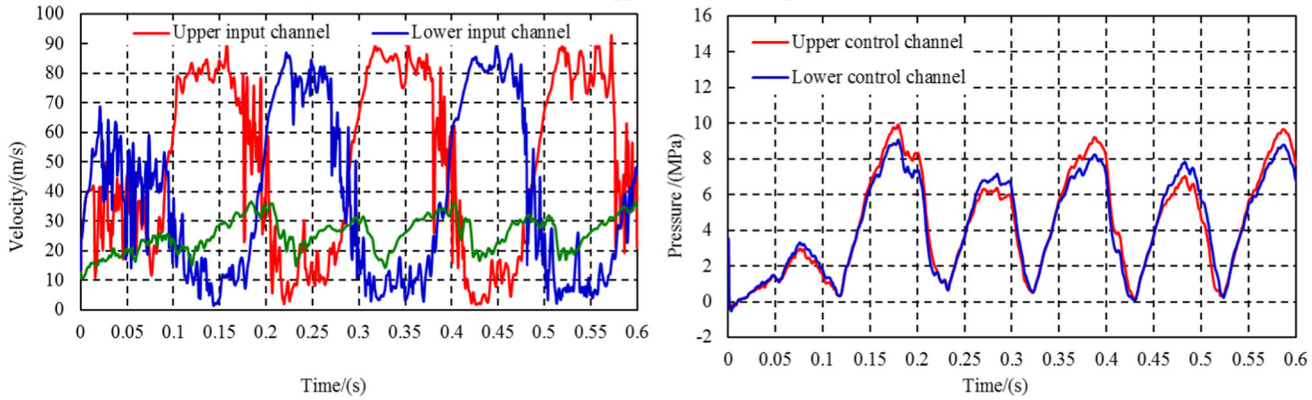

(b) Flow characteristic curve of upper and lower control channels

Fig. 11 Fluid flow characteristic curve of inlet flow rates (25L/s)

Fig. 12 Experimental test system

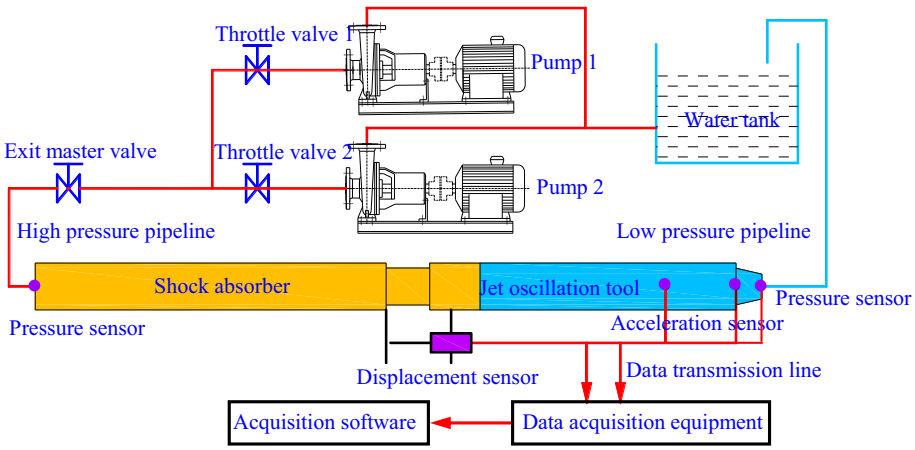

Fig. 13 Experimental test of non-moving component jet oscillation tool

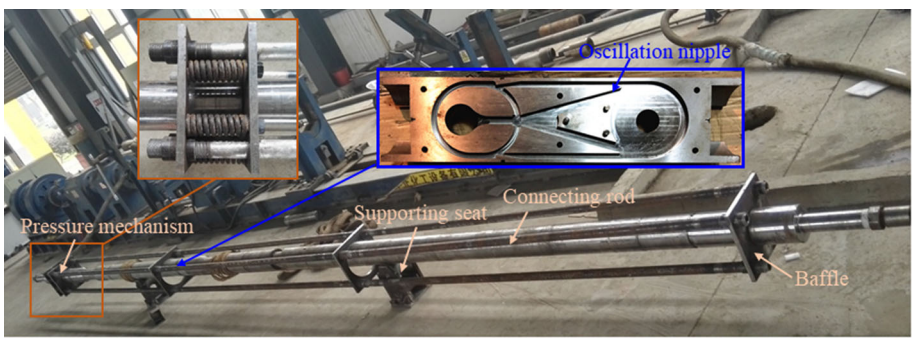

Table 2 Experimental conditions

Flow rate (L/s)	5	9	21	25
Flow rate (m^3/h)	18.00	32.40	75.59	90.00
Pressure (MPa)	0.27	0.89	5.41	7.90
Density (kg/m^3)	998.2			
Dynamic viscosity (Pa·s)	0.001			

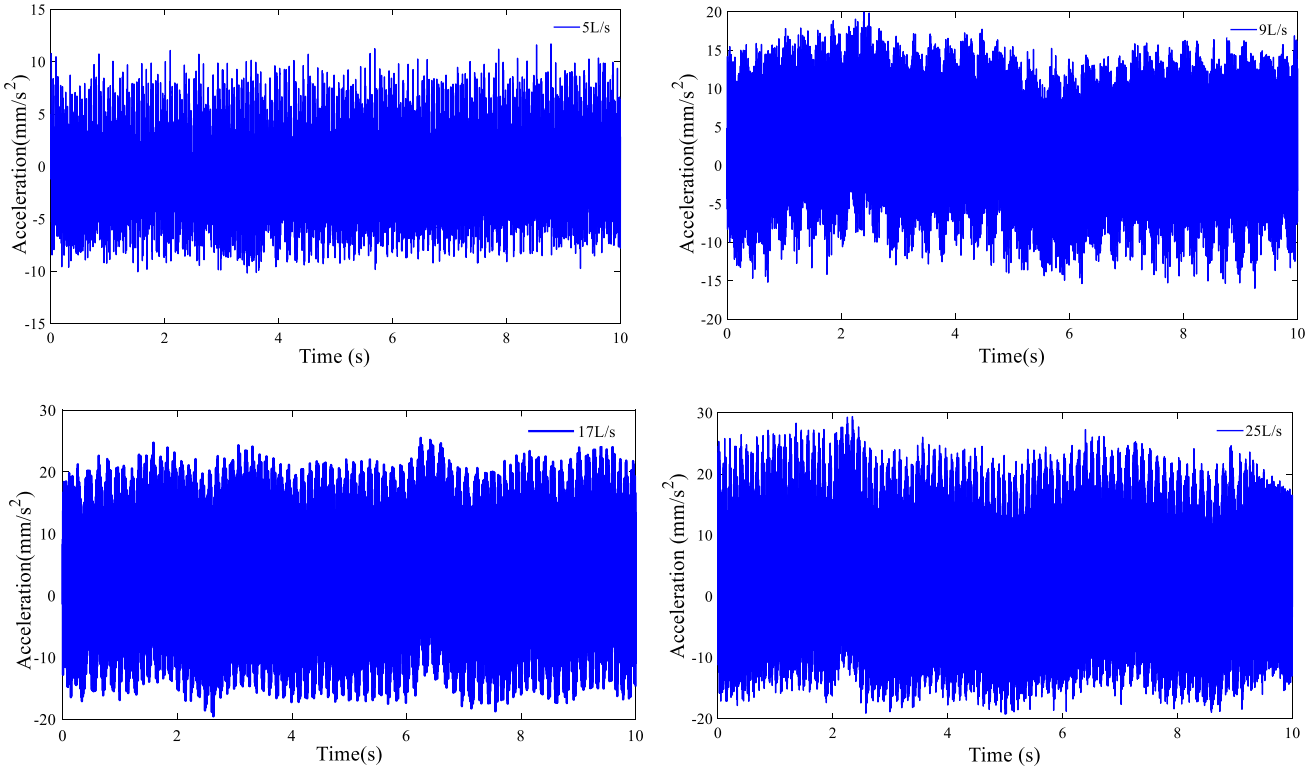

Fig. 14 Acceleration signal test results under different input flow conditions

collected and shown in Fig. 14. In experimental tests, the tool can regularly work with all quantities of flow rates, and a periodical vibration is generated. When the input flow rate is 5L/s, the acceleration variation range is -8 ~ 10 mm/s^2. As the input flow increases, the vibration amplitude of the acceleration increases continuously and the vibration test waveform appears in the acceleration test result. When the input flow rate is increased to 25L/s, the acceleration range can reach -18 ~ 25 mm/s^2.

The pressure sensors are installed at the connect location between high and low pressure pipelines and the tool to perform pressure change tests at the inlet and outlet end. Each time the flow rate is adjusted, and after the jet oscillation works smoothly, the pressure data collection is performed by data acquisition equipment. The average working pressure loss can be obtained from average value of the pressure at inlet and outlet by using computer. The characteristic curve of the pressure loss is obtained and the comparison

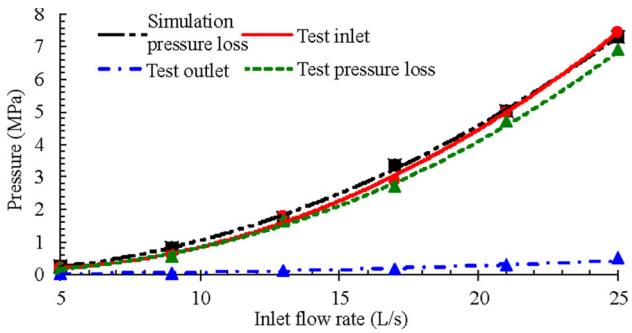

Fig. 15 Characteristic curve of pressure loss of experiment and simulation results

analysis with the numerical simulation results is completed, which is shown in Fig. 15. The pressure loss obtained by the experimental test is basically consistent with the trend of the simulation result with the change of the inlet flow. The maximum pressure loss of simulation is 7.32 MPa and the

minimum pressure loss is 0.25 MPa. The maximum pressure loss of experimental test is 6.93 MPa and the minimum pressure loss is 0.23 MPa. When the inlet flow rate is 5, 9, 17, 25 L/s, the difference values between simulation results and experimental results are 0.02, 0.07, 0.27, 0.48 MPa. The errors are 8, 8.4, 8, 6.6%. With the increase in flow rate, the errors of experiment and simulation are always within reasonable range.

6 Conclusions

Aiming at the problems of high drilling friction and serious backing pressure on the drill string under the difficult oil and gas drilling conditions, a non-moving component jet oscillation tool is proposed. The vibrations generated by this tool can change the friction status between drill string and borehole wall, such as static to dynamic friction, and improve drilling efficiency.

Combining the field working conditions, the numerical simulations of the internal flow are completed, and the wall-attached and switching behaviors complete periodically in the oscillator. With the inlet flow increasing, the fluid velocities at the inlet and outlet locations show quasi-linear distributions, and the fluid pressures loss changes periodically. The inlet flow rate increases from 5 to 25L/s, and the inlet velocity increases from 1.27 to 6.37 m/s. The periodic pressure pulse is generated, and the initial deflection time of the jet flow is depended on design parameters, so as the fluid switching period.

Through the experimental test, the internal characteristics of this tool are obtained. As the inputting flow increases, the amplitude of the vibration acceleration increases continuously. With the inlet flow increase, the experimental and simulation results are basically consistent. The maximum pressure loss of simulation result is 7.32 MPa and the minimum pressure loss is 0.25 MPa. The maximum pressure loss of experimental test is 6.93 MPa and the minimum pressure loss is 0.23 MPa. With the increase in flow rate, the errors of experiment and simulation are always within reasonable range.

Acknowledgements This work is supported by State Key Laboratory of Gas Disaster Monitoring and Emergency Technology, China (2021SKLKF07), and the Science and Technology Innovation Fund, Chengdu, China (2022-RCO3-00005-CG).

References

1. Xiaowei, G.; Wei, Li.; Zhongshan, Q., et al.: A research status and difficulties of unconventional oil and gas exploration technology in china. Chin. Manganese Ind. **35**(03), 108–111 (2017)
2. Pehlivantürk, C.; Chen, D.; Ashok, P., et al.: Path advisory for slide drilling using a nonlinear wellbore propagation model and genetic algorithm. J. Petrol. Sci. Eng. (2019). https://doi.org/10.1016/j.petrol.2019.03.080
3. Wei, W.; Zhichuan, G.; Wenzhe, Z., et al.: Analysis of factors influence drill string extending ability in horizontal well drilling. Drill Prod Technol **38**(02), 9–13 (2015)
4. Changjin, W.; Zifeng, Li.; Yinpeng, Li., et al.: Experiment on the rotation of compressional bucking column in the liquid-filled cylinder. ACTA PETROLEI SINICA **39**(03), 341–348 (2018). https://doi.org/10.7623/syxb201803010
5. Cayres, B.; da Fonseca, C.; Santos, A., et al.: Analysis of dry friction-induced stick-slip in an experimental test rig modeling a drill string. In Proceedings of the 9th IF To MM International Conference on Rotor Dynamics. Springer, Cham, pp 195–204. (2015). https://doi.org/10.1007/978-3-319-06590-8_16
6. Tian, J.L.; Hu, S.H.; Li, Y., et al.: Vibration characteristics analysis and experimental study of new drilling oscillator. Adv. Mech. Eng. **8**(6), 1–10 (2016). https://doi.org/10.1177/1687814016652090
7. Sarker, M.; Rideout, D.G.; Butt, S.D.: Dynamic model for longitudinal and torsional motions of a horizontal oil well drill string with wellbore stick-slip friction. J. Petrol. Sci. Eng. **150**, 272–328 (2017). https://doi.org/10.1016/j.petrol.2016.12.010
8. Tian, J.L.; Yang, Z.; Li, Y., et al.: Vibration analysis of new drill string system with hydro-oscillator in horizontal well. J. Mech. Sci. Technol. **30**(6), 2443–2451 (2016). https://doi.org/10.1007/s12206-016-0504-z
9. Tian, J.L.; Yang, Y.L.; Dai, L.M.; Lin, X.Y.: Kinetic characteristics analysis of a new torsional oscillator based on impulse response. Arch. Appl. Mech. **88**(10), 1877–1891 (2018). https://doi.org/10.1007/s00419-018-1412-8
10. Rasheed, W.: Extending the reach and capability of non-rotating BHAs by reducing axial friction. SPE 68505. (2001) https://doi.org/10.2118/68505-MS.
11. Newman, K.; Burnett, T.; Pursell, J., et al.: Modeling the affect of a downhole vibrator. SPE 121752. (2009) https://doi.org/10.2118/121752-MS.
12. Al-Buali, M.H.; Dashash, A.A.; Shawly, A.S., et al.: Maximizing coiled tubing reach during logging extended horizontal wells using E-line Agitator. SPE 127399. (2009) https://doi.org/10.2118/127399-MS.
13. Barton, S.; Baez, F.; Alali A.: Drilling performance improvements in gas shale plays using a novel drilling agitator device. SPE 144416. (2011) https://doi.org/10.2118/144416-MS.
14. Li, Z.F.; Yang, H.B.; Xu, C.T., et al.: Bit feed principles and technologies in slide-drilling directional wells. Nat. Gas. Ind. **33**(12), 94–98 (2013). https://doi.org/10.1016/j.petrol.2017.01.054
15. Dong, X.C.; Xiong, J.Y.; Wang, G.H., et al.: Study on running characteristic of oscillation impacter for oil-drilling. J. Mech. Eng. **50**(21), 197–205 (2014). https://doi.org/10.3901/JME.2014.21.197
16. Wang, P.; Ni, H.J.; Wang, R.H., et al.: Influence laws of modulated vibration on friction reduction in inclined-wells. J. Chin. Univ. Petrol. **38**(4), 93–97 (2014). https://doi.org/10.3969/j.issn.1673-5005.2014.04.013
17. Gee, R.; Hanley, C.; Hussain, R., et al.: Axial oscillation tools vs. lateral vibration tools for friction reduction-what's the best way to shake the pipe. SPE173024. (2015) https://doi.org/10.2118/173024-MS.
18. Panda, P.P.; Busari, O.; Lucht, R.P., et al.: Effect of the nature of vitiated crossflow on the flow-field of a transverse reacting jet. Exp. Fluids **58**(2), 9 (2017). https://doi.org/10.1007/s00348-016-2288-4
19. Tian, J.L.; Yang, Y.L.; Dai, L.M., et al.: Dynamic mechanism of fluidic oscillation of a new friction reducing tool. Nat. Gas. Ind. **39**(5), 85–92 (2019). https://doi.org/10.3787/j.issn.1000-0976.2019.05.012

20. Hsu, C.M.; Jhan, W.C.; Chang, Y.Y.: Flow and heat transfer characteristics of a pulsed jet impinging on a flat plate. Heat Mass Transf. pp 1–18. (2019) https://doi.org/10.1007/s00231-019-02696-w.
21. Hou, S.; Cao, Y.H.: Calculation of surface heat transfer coefficient based on Reynolds-averaged Navier-Stokes equations. J. Aerosp. Power **30**(6), 1319–1327 (2015)
22. Chang, S.P.; Wang, Y.S.: Prediction of waterjet performance using k–ε turbulence models. J. Huazhong Univ. of Sci. Tech. (Natural Science Edition) **40**(04), 88–90 (2012)
23. Fu, C.B.; Song P.Y.: Discussion on critical reynolds number of fluid film flow state between the non-contact mechanical seal faces. Lubrication and Sealing, pp 63–68+77. (2019)
24. Orlandi, P.: Turbulent kinetic energy production and flow structures in flows past smooth and rough walls. J. Fluid Mech. (2019). https://doi.org/10.1017/jfm.2019.96
25. He, J.F.; Yin, K.: Design and feasibility analysis of a fluidic jet oscillator with application to horizontal directional well drilling. J. Nat. Gas Sci. Eng. **27**(03), 1723–1731 (2015)